

# Drop-on-Demand Inkjet Printing of Thermally Tunable Liquid Crystal Microlenses

Ellis Parry,<sup>1, a)</sup> Serena Bolis,<sup>1, 2, 3</sup> Steve J. Elston,<sup>1</sup> Alfonso A. Castrejón-Pita,<sup>1, b)</sup> and Stephen M. Morris<sup>1, c)</sup>

<sup>1)</sup>*Department of Engineering Science, University of Oxford, Parks Road, Oxford, OX1 3PJ, UK*

<sup>2)</sup>*OPERA-Photonics Group, Université libre de Bruxelles, 50 Avenue F.D.Roosevelt CP 194/5 1050 Bruxelles, Belgium*

<sup>3)</sup>*ELIS Department, Gent Universiteit, Technologiepark-Zwijnaarde 15, 9052 Gent, Belgium*

**Keywords:** liquid crystals, inkjet printing, microlenses, microfabrication

In this letter, we demonstrate Drop-on-Demand printing of variable focus, polarisation-independent, liquid crystal (LC) microlenses. By carefully selecting the surface treatment applied to a glass substrate, we are able to deposit droplets with a well-defined curvature and contact angle, which result in micron-sized lenses with focal lengths on the order of  $300\mu\text{m}$  -  $900\mu\text{m}$ . Observations with an optical polarising microscope confirm the homeotopic alignment of the LC director in the droplets, which is in accordance with the polarisation independent focal length. Results show that microlenses of different focal lengths can be fabricated by depositing successive droplets onto the same location on the substrate, which can then be used to build up programmable and arbitrary arrays of microlenses of various lens sizes and focal lengths. Finally, we utilise the thermal dependency of the order parameter of the LC to demonstrate facile tuning of the focal length. This technique has the potential to offer a low-cost solution to the production of variable focus, arbitrary, microlens arrays.

Microlens arrays are fundamental micro-optical components used in a wide variety of imaging, sensing and optical communications applications.<sup>1</sup> Due to their small geometric profile and optical properties, microlenses are perfectly suited to light collection applications where space is limited; for example, they are commonly found in CCD cameras, photovoltaic cells and fibre optic bundles. Historically, microlens arrays have been manufactured using multi-step processes such as photolithography, reflow-melting and hot-embossing.<sup>2-4</sup> Although highly scalable, these techniques are limiting with respect to the range of compatible materials and possible substrate geometries. Moreover, these techniques often require a master lens array template which can increase the cost and complexity in the ad-hoc fabrication of bespoke microlens arrays.<sup>5</sup>

More recently, simple and efficient manufacturing methods have emerged in the fabrication of microlenses, which allow the use of different materials and give greater freedom with regards

to the choice of substrates and array patterns. One such technique is Drop-on-Demand (DoD) inkjet printing, which is already firmly established in the fields of graphical printing, additive manufacturing and printed electronics.<sup>6,7</sup> The technique is particularly attractive as it is a digitally controlled, precise, scalable and highly cost-effective additive manufacturing process. This has led to inkjet printing being considered as an alternative fabrication technique in a range of fields such as the display, pharmaceutical and bioengineering industries.<sup>8-11</sup> The precision jetting of UV-curable optical polymers to form in-situ fixed-focus microlenses has been widely demonstrated in recent years and it has since become a key technology in the production of cost-effective microlens arrays.<sup>6,12,13</sup> Recently, the inkjet printing of more complex fluids such as liquid crystals (LCs) has been demonstrated, for use as optical sensors and in the fabrication of printable optically-pumped thin film lasers.<sup>14,15</sup>

However, DoD inkjet printing has yet to be applied to the fabrication of variable focus microlenses. A variable focus microlens has the ability to change the focal distance without the use of multiple lens systems or mechanical displacement. This has the effect of reducing the number of components required during man-

---

<sup>a)</sup>ellis.parry@eng.ox.ac.uk

<sup>b)</sup>alfonso.castrejon-pita@wadham.ox.ac.uk

<sup>c)</sup>stephen.morris@eng.ox.ac.uk

ufacturing and allows smaller and more compact devices to be produced. Current methods for achieving a tunable microlens include liquid filled elastic lenses, gradient refraction index (GRIN) and LC lenses.<sup>16,17</sup> Liquid-filled lenses rely on complex microfluidic systems to deform the lens surface and subsequent focussing properties. LC microlenses are an attractive alternative due to the ability of the LC molecules to reorientate in the presence of externally applied stimuli; this results in a change in the refractive index and consequent focussing properties without any mechanical deformation of the lens profile or the need for complex microfluidic control.<sup>18</sup> Nevertheless, such lenses are typically formed either by applying a complex electric field to a LC cell, to induce a gradient in the refractive index,<sup>19</sup> or via filling the LC between a treated glass substrate and a fixed lens array.<sup>20</sup> Due to the complex fabrication procedures required to form such lenses, they are not readily compatible with low-cost, highly scalable manufacturing processes such as printing.

In this work, we demonstrate DoD inkjet printing of LC microlenses that exhibit focal lengths of a few 100 microns. To obtain sessile droplets with a plano-convex geometrical configuration after deposition onto the substrate, we coat glass surfaces with a homeotropic polymer layer. As a result, the lenses are polarisation independent, due to the uniform alignment of the director throughout the droplet. This is desirable as it eliminates the need for additional polarisation control elements, which can significantly reduce the optical efficiency of a system. Furthermore, the focal length of the lens can be selected by forming larger lenses via the subsequent deposition of individual droplets onto the same location on the substrate. Finally, the variable focus potential of the lenses is demonstrated through the aid of thermal tuning.

Microlens arrays were formed using the experimental set-up shown in **Figure 1a**. The print-head used was a MJ-ABP-01-70 dispenser (Microfab Technologies inc) with a  $70\mu\text{m}$  nozzle diameter. A nematic LC (E7, Merck KGaA) was used as the functional ink, which is supplied to the dispenser via PTFT tubing and a static pressure syringe pump. A custom-made heating sleeve, with a DBK-HPOS 20W heating element (DBK Enclosures) and K-type thermocouple, was used to control the temperature of the print-head. A printing temperature of  $60^\circ\text{C}$  was chosen in order to raise the LC above the clearing temperature,  $T_c$  ( $58^\circ\text{C}$ ). At this temperature, the bulk viscosity of the fluid is reduced from  $0.75\text{gcm}^{-2}$  to approximately

$0.15\text{gcm}^{-2}$ , sufficient to deposit the LC using inkjet printing. Additionally, at this temperature, the anisotropic components of the viscosity disappear, leading to increased homogeneity in the droplet properties.

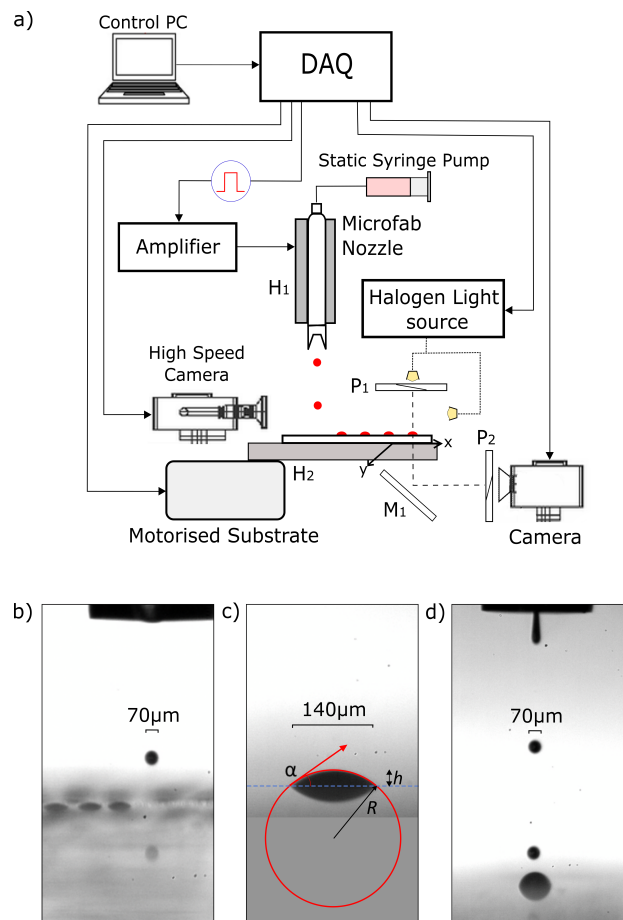


FIG. 1. a) Schematic showing the experimental layout used to print liquid crystal microlenses.  $P_1$  and  $P_2$  are linear polarisers,  $H_1$  and  $H_2$  are the nozzle and substrate heating elements respectively and  $M_1$  is a mirror. b), c) and d) Show high-speed images (15,000fps, 8/ $\mu\text{s}$  exposure time) taken during the printing process. b) An array of homogeneous LC microlenses being printed. c) Example of a single sessile drop with a plano-convex profile (reflection of the glass substrate can also be seen). The radius of curvature is defined as  $R$ , contact angle as  $\alpha$  and droplet height as  $h$ . d) Formation of a larger droplet by printing multiple droplets onto the same location.

Drop formation at the nozzle and deposition onto the substrate was captured using the combination of a high-speed Phantom V12.1 camera and a halogen high-intensity white light source (OSL2 3200K, Thorlabs) arranged in a shadowgraphy configuration. The director profile of the LC droplet 10ms after deposition onto

the substrate was interrogated using a colour camera (DFK 23U274, The Imaging Source) with linear polarisers that were placed before and after the LC sample with the transmission axes crossed. Accurate positioning of the droplet was achieved via a custom-made x-y motorised stage. A separation of  $600\mu\text{m}$  between the nozzle and the printing substrate allowed both drop formation and impact to be visualised simultaneously. Timing synchronisation, temperature control and printing specifications were achieved via a LabVIEW program and DAQ card (NI USB-6351, National Instruments).

The criteria for successful LC lens formation is a stable droplet boundary, uniform alignment of the LC director and repeatability of the printed volume. The first two conditions depend on the substrate properties, whilst the third relies on the printing reliability. For this study we used a Nissan (SE4811) polymer coated glass slide, held at  $25^\circ\text{C}$ , as the printing substrate. The surface was chosen such that each droplet does not spread excessively on contact and exhibits strong homeotropic anchoring. Figure 1b shows high-speed images of a LC droplet being deposited. The impact velocity of the droplet was  $1.5\text{ms}^{-1}$ , which given the fluid properties, is well below the point at which splashing may occur.<sup>21</sup> After impact with the printing surface, equilibrium of the LC droplet diameter and contact angle  $\alpha$  is reached in under  $10\text{ms}$ , with no observable hysteresis. The effects of gravity on the printing process can be quantified using the Bond number  $Bo = \frac{\rho g h^2}{\sigma}$ , where  $\rho$  is the density of the LC,  $g$  is the acceleration due to gravity,  $h$  is the droplet height and  $\sigma$  is the surface tension of the LC. For  $Bo \ll 1$  gravitational effects can be assumed to be negligible, which in our system required droplet diameters to be less than  $1\text{mm}$ . Since the effects of gravity on droplet shape are negligible, the free surface energy is dominated by the contribution from surface tension. The droplet thus assumes the shape of a spherical cap of radius  $R$  to minimise its free surface energy, as seen in Figure 1c. The focal length  $f$  of a plano-convex microlens in air is given by the equation:  $f = \frac{R}{n-1}$ . Evidently, the focal length  $f$  can be selected by changing either the radius of curvature  $R$  or the refractive index  $n$  of the lens material.

Printing of the LC must be precise enough to produce droplets of homogeneous volume. At the selected printing temperature, a single uniform droplet with a diameter of  $70\mu\text{m}$ , a volume of  $180\text{pL}$ , was reliably produced for each posi-

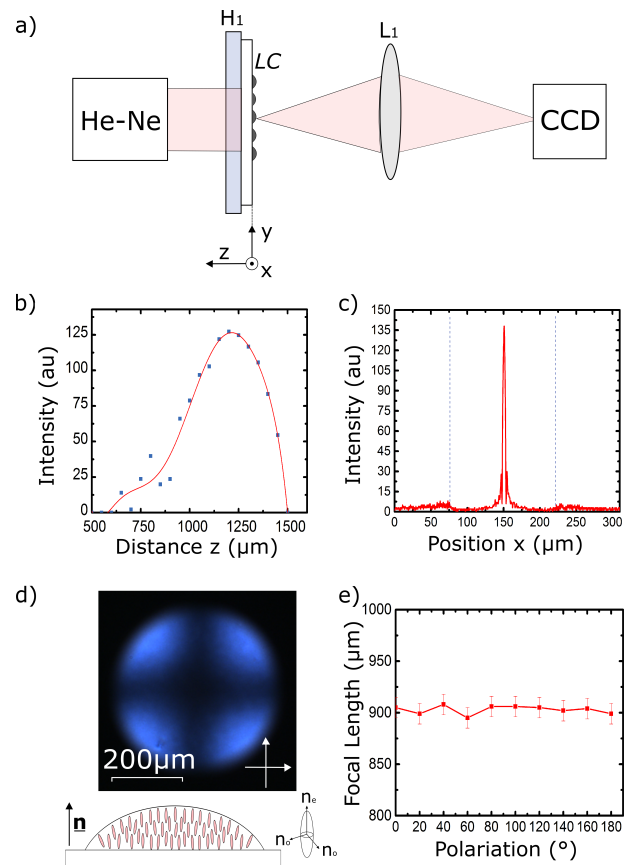


FIG. 2. a) The optical set-up for determining the focal length of the microlens arrays, where  $L_1$  is a convex lens with a fixed focal length of  $25\text{mm}$ ,  $H_1$  is a heating element and  $LC$  is the liquid crystal microlens array. b) Shows the variation in the light intensity of the focal spot of a  $390\mu\text{m}$  diameter lens as it is moved in the positive  $z$ -direction. c) The intensity cross-section at the focal plane of a  $140\mu\text{m}$  diameter lens, the dotted lines indicate the corresponding position of the lens perimeter. d) Polarised microscopy image of a single microlens with a schematic of the LC director profile within the droplet. The LC director is given by the unit vector  $\mathbf{n}$ , whilst  $n_o$  and  $n_e$  are respectively the ordinary and extraordinary refractive index axes, relative to the orientation of a LC molecule. e) The focal length of a single  $310\mu\text{m}$  diameter microlens as a function of the orientation of incident linearly polarised light.

tive square pulse (drop-on-demand push-mode operation), supplied via the associated Microfab software. Subtle changes to the droplet diameter can be achieved by increasing the duration of the waveform. However, for longer waveforms, spontaneous break-up of the fluid ligament can occur as it exits the nozzle, resulting in undesirable satellite droplets being produced. This instability limits the droplet diameter to approximately that of the nozzle size

(70 $\mu\text{m}$ ). More pronounced changes in the volume of the resulting lens were instead achieved by printing multiple droplets onto the same location, as demonstrated in Figure 1d.

The focal length of the microlenses fabricated in this study were investigated using the optical arrangement shown in **Figure 2a**. A continuous wave He-Ne laser ( $\lambda = 632.8\text{nm}$ ) was used to illuminate the sample. Initially, the lens  $L_1$  and CCD were positioned such that an in-focus image of the LC lens substrate surface was formed at the CCD ( $z = 0$ ). A series of images were then taken as the LC microlens array was translated in the positive  $z$ -direction. A maximum in pixel intensity was observed when the microlens array was translated such that the CCD and lens  $L_1$  formed an image of the focal spot of the LC microlens ( $z = f_{LC}$ ). The pixel intensities were then plotted as a function of the distance,  $z$ , for the image sequence. The position of the maximum of this plot was then used to estimate the focal length,  $f_{LC} \pm 10\mu\text{m}$ , to within an accuracy of  $10\mu\text{m}$ , as seen in Figure 2b. Figure 2c shows an example of the variation in intensity along the  $x$ -direction of a  $140\mu\text{m}$  diameter lens at the focal plane and demonstrates good focussing properties with an optical transmission of 74%, comparable to other LC microlenses.<sup>17</sup>

In our system, both the surface of the printing substrate and the LC air interface impose homeotropic anchoring conditions on the LC droplet. Figure 2d shows an optical polarised microscope image of a LC microlens along with a schematic of the LC director configuration. The dark cross on the microscope image, which follows the polarisation axes, implies homeotropic alignment of the LC director throughout the depth of the lens. However, the blue regions of the image indicate a degree of birefringence which results from the slight tilt of the LC director, which is induced by the upper curved interface. The effect of this tilt on the focussing properties of the microlens is indiscernible due to the curvature being present only at the edges of the lens and at the top interface, with a maximum deviation from homeotropic alignment being equal to the contact angle,  $\alpha$ . Collimated incident light will interact predominantly with the ordinary component of the refractive index  $n_o$ . Due to symmetry of the director profile, the focussing properties of the microlens will be constant for light that is normal to the lens plane, regardless of its polarisation state. This is exemplified in Figure 2e which shows the focal length of a single  $420\mu\text{m}$  diameter lens as a function of the orientation of linearly polarised incident light.

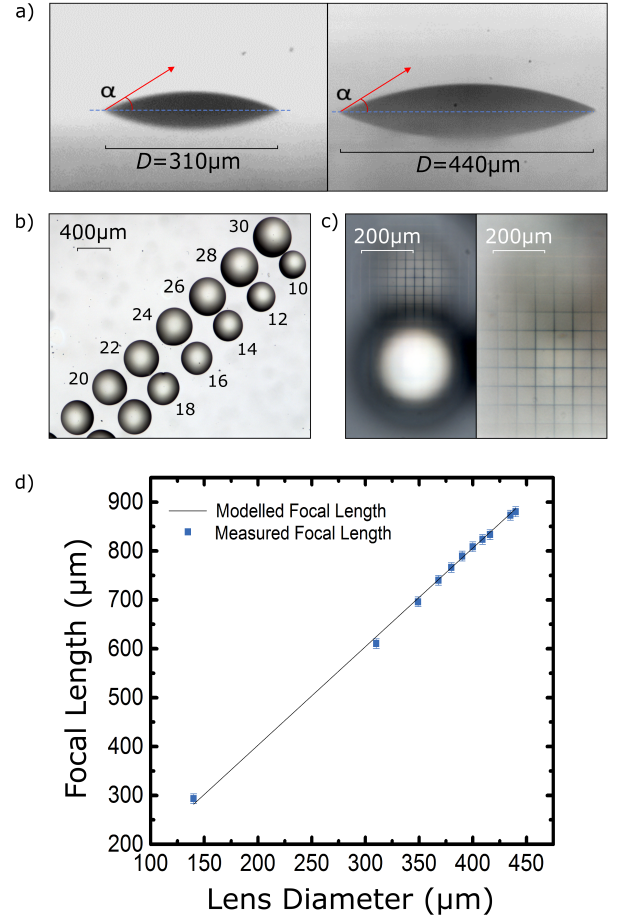


FIG. 3. a) High speed camera images of two spherical plano-convex lenses with different droplet diameters  $D$ , but the same contact angle,  $\alpha$ . b) Microscope image with uncrossed polarisers of an array consisting of microlenses of different diameters. The numbers indicate the number of individual droplets printed in each microlens. c) Optical polarising microscopy images showing the real image formed of a  $25\mu\text{m}$  spacing grid placed under two lenses of different diameters. The left image is focussed at the image plane for the smaller lens with a focal length of  $610\mu\text{m}$ , whereas the right image is focussed at the larger lens image plane with a focal length of  $880\mu\text{m}$ . d) Focal length as a function of the diameter of a microlens. The solid line represents the results for a perfectly spherical lens with a constant refractive index.

The contact angle  $\alpha$  results from the balance of interfacial tension between the substrate, fluid and surrounding air, thus it is independent of lens volume. This results in a constant contact angle of  $28.5^\circ$ , as seen in **Figure 3a**. The  $f$ -number ( $N = \frac{f}{D}$ ) is a dimensionless parameter which characterises the ability of a lens to collect light, with lower  $f$ -numbers correspond-



ing to more efficient light collection. As the diameter of a spherical cap ( $D$ ) is proportional to its radius of curvature and corresponding focal length, the  $f$ -number of lenses printed on the same substrate with the same fluid will be constant, regardless of diameter. In our configuration this resulted in a relatively low  $f$ -number of  $N = 2$ , which is comparable to that of glass and plastic microlenses used in light collection applications that have been produced using techniques such as photolithography and resist melting.<sup>22</sup>

A printed array of microlenses of different diameters, produced in a single sequence, is shown in Figure 3b, the numbers accompanying each lens correspond to the number of constituent droplets printed to form each lens. The difference in focal length is emphasised in Figure 3c, which shows microscope images of the real image formed of an underlying  $25\mu\text{m}$  grid, placed  $2\text{mm}$  below the lens plane. The smaller lens in Figure 3c was formed by printing 10 droplets onto the same position at a print frequency of  $3.5\text{kHz}$  resulting in a focal length of  $610 \pm 10\mu\text{m}$ . The right hand image of Figure 3c shows the in-focus image of the larger lens, produced in the same manner, but with 30 droplets and with a larger focal length of  $880 \pm 10\mu\text{m}$ . The in-focus image is formed at a greater distance from the lens plane and with two times higher magnification.

To investigate the degree of correlation between droplet volume and focal length, we compared the measured focal length (using the method outlined in Figure 2c) to the focal length calculated for a perfectly spherical plano-convex lens with the same physical dimensions and a single uniform refractive index that is equivalent to the ordinary refractive index for the nematic LC, E7 determined at  $632.8\text{nm}$  ( $n_o = 1.52$ ). As shown in Figure 3d the experimental data are in strong agreement with the modelled focal length. This suggests that the radius of curvature of the lens is indeed governed by the droplet volume and is consistent with what we would expect for a spherical cap. Additionally, the strong agreement confirms that the small tilt imposed on the LC director (Figure 2d) does not noticeably affect the focussing properties of the lens.

To assess the tunability of the microlenses, we measured the focal length over a range of temperatures using the method described in Figure 2a. The experimental data for a single lens were compared to the focal length of a lens with a uniform refractive index equal to  $n_o$  of E7, taking into account the temperature dependency,<sup>23</sup> and constant dimensions

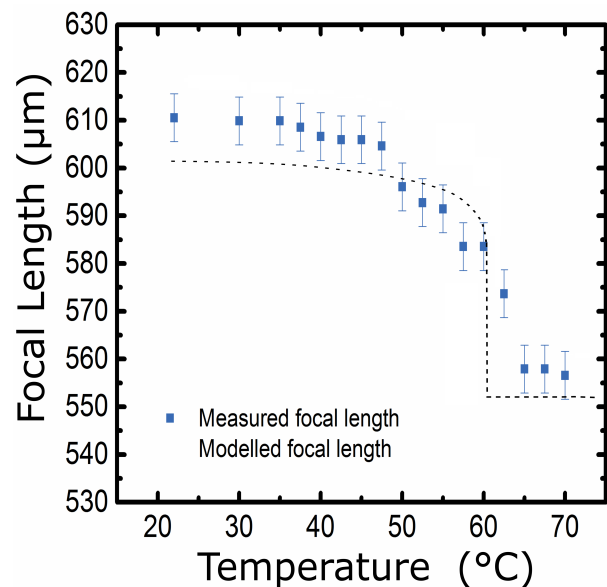


FIG. 4. The focal length of a single microlens as a function of temperature. The modelled focal length was calculated using a uniform refractive index equal to that of E7 over a range of temperatures and using lens dimensions consistent with the printed lens being compared.

equal to that of the printed LC microlens. As seen in **Figure 4**, the experimentally determined focal length decreases as a function of temperature and closely follows the modelled data, which take into account the increase of the refractive index  $n_o$  caused by the temperature dependency of the order parameter of the LC. The droplet boundary was also measured as the temperature was changed to assess whether any change in the contact angle and droplet boundary was observed. No observable change in droplet boundary or profile was noted, indicating the decrease in focal length was due to the decrease in the order parameter of the LC as it approached the isotropic phase. It can be seen that for a change in temperature of  $40^\circ\text{C}$ , the focal length changes by  $60\mu\text{m}$ , however, the majority of this change happens within  $15^\circ\text{C}$  of the clearing temperature.

## CONCLUSION

In summary, through a combination of surfactant and deposition conditions, we have demonstrated the drop-on-demand inkjet printing of nematic LCs that naturally form sessile droplets upon impact with the substrate. These droplets behave as polarization independent microlenses that can be readily deposited into bespoke,

pre-programmable arrays with a variety of focal lengths. We show results for microlenses with diameters ranging from 140 to 880  $\mu\text{m}$  and  $f$ -numbers of 2. Further, the focal length of these LC microlenses can be thermally tuned over 10's of microns, which would be of importance for applications requiring passive focussing elements. Future work will involve the encapsulation and stabilisation of such lenses.

## ACKNOWLEDGEMENTS

E.P. acknowledges the financial support from EPSRC and Merck for a CASE Studentship. S.M.M. and A.A.C.P thank the Royal Society for the financial support. S.B. thanks the Fondation Philippe Wiener - Maurice Anspach, the Fund for Research Training in Industry and Agriculture (FRIA) and the Fonds David et Alice Van Buuren and the Fondation Jaumotte-Demoulin.

- <sup>1</sup>T. Hou, C. Zheng, S. Bai, Q. Ma, D. Bridges, A. Hu and W. W. Duley, *Appl. Opt.*, 2015, **54**, 7366–7376.
- <sup>2</sup>M.-H. Wu, C. Park and G. Whitesides, *Langmuir*, 2002, **18**, 9312–9318.
- <sup>3</sup>N. Ong, Y. Koh and Y. Fu, *Microelectronic Engineering*, 2002, **60**, 365–379.
- <sup>4</sup>D. Daly, R. F. Stevens, M. C. Hutley and N. Davies, *Measurement Science and Technology*, 1990, **1**, 759.
- <sup>5</sup>H. Becker and U. Heim, *Sensors and Actuators A: Physical*, 2000, **83**, 130 – 135.
- <sup>6</sup>P. Calvert, *Chemistry of Materials*, 2001, **13**, 3299–3305.
- <sup>7</sup>H. S. Kim, J. S. Kang, J. S. Park, H. T. Hahn, H. C. Jung and J. W. Joung, *Composites Science and Technology*, 2009, **69**, 1256–1264.
- <sup>8</sup>D. J. Hayes, W. R. Cox and M. E. Grove, *Journal of the Society for Information Display*, 2001, **9**, 9–13.
- <sup>9</sup>B.-J. De Gans, P. Duineveld and U. Schubert, *Advanced Materials*, 2004, **16**, 203–213.
- <sup>10</sup>J. R. Castrejón-Pita, W. Baxter, J. Morgan, S. Temple, G. D. Martin and I. M. Hutchings, *Atomization and Sprays*, 2013, **23**, 571–595.
- <sup>11</sup>R. D. Boehm, P. R. Miller, J. Daniels, S. Stafslie and R. J. Narayan, *Materials Today*, 2014, **17**, 247 – 252.
- <sup>12</sup>D. b. MacFarlane, V. b. Narayan and J. b. Tatum, *IEEE Photonics Technology Letters*, 1994, **6**, 1112–1114.
- <sup>13</sup>J. Y. Kim, K. Pfeiffer, A. Voigt, G. Gruetzner and J. Brugger, *J. Mater. Chem.*, 2012, **22**, 3053–3058.
- <sup>14</sup>N. Herzer, H. Guneyasu, D. J. D. Davies, D. Yildirim, A. R. Vaccaro, D. J. Broer, C. W. M. Bastiaansen and A. P. H. J. Schenning, *Journal of the American Chemical Society*, 2012, **134**, 7608–7611.
- <sup>15</sup>D. J. Gardiner, W.-K. Hsiao, S. M. Morris, P. J. W. Hands, T. D. Wilkinson, I. M. Hutchings and H. J. Coles, *Soft Matter*, 2012, **8**, 9977–9980.
- <sup>16</sup>C. Monat, P. Domachuk and B. J. Eggleton, *Nat Photon*, 2007, **1**, 106–114.
- <sup>17</sup>S. Xu, Y. Li, Y. Liu, J. Sun, H. Ren and S.-T. Wu, *Micromachines*, 2014, **5**, 300–324.
- <sup>18</sup>D.-K. Yang and S.-T. Wu, *Fundamentals of Liquid Crystal Devices*, 2006, pp. 1–378.
- <sup>19</sup>T. Nose and S. Sato, *Liquid Crystals*, 1989, **5**, 1425–1433.
- <sup>20</sup>H. T. Dai, Y. J. Liu, X. W. Sun and D. Luo, *Opt. Express*, 2009, **17**, 4317–4323.
- <sup>21</sup>C. Josserand and S. Thoroddsen, *Annual Review of Fluid Mechanics*, 2016, **48**, 365–391.
- <sup>22</sup>H. Ottevaere, R. Cox, H. P. Herzig, T. Miyashita, K. Naessens, M. Taghizadeh, R. Vlkel, H. J. Woo and H. Thienpont, *Journal of Optics A: Pure and Applied Optics*, 2006, **8**, S407.
- <sup>23</sup>J. Li, C.-H. Wen, S. Gauza, R. Lu and S.-T. Wu, *Journal of Display Technology*, 2005, **1**, 51–61.